One neutron pickup reactions in the $^{32}S + ^{144}Sm$ and $^{32}S + ^{166}Er$ systems at energies close to the Coulomb barrier

D. Tomasi, J. O. Fernández Niello, A. O. Macchiavelli, A. J. Pacheco, J. E. Testoni, D. Abriola, O. A. Capurro, D. E. Di Gregorio, M. di Tada, C. P. Massolo,* and F. Penayo
Laboratorio TANDAR, Departamento de Física, Comisión Nacional de Energía Atómica, Avenida del Libertador 8250, 1429 Buenos Aires, Argentina
(Received 27 April 1993)

One neutron transfer cross sections in the systems $^{32}S + ^{144}Sm$ and $^{32}S + ^{166}Er$ have been measured at energies close to the Coulomb barrier. Mass and charge identification was achieved using characteristic x rays. Transfer probabilities were analyzed by considering barrier penetration mechanisms. Possible enhancement effects due to permanent quadrupole deformations are investigated and compared with the experimental results.

PACS number(s): 25.70.Hi, 21.10.Gv, 27.70.+q

I. INTRODUCTION

The study of the interaction of heavy nuclei at energies close to the Coulomb barrier has shown spectacular effects due to the nuclear static deformation of one or both of the reaction partners. The origin of these deformation effects, which reflect in an enhancement of the fusion and transfer rates, can be understood as stemming from the approach of the nuclear surfaces at orientation angles in the vicinity of the poles for a fixed bombarding energy.

The role of the quadrupole deformation in the enhancement of transfer cross sections has been investigated using samarium isotopes [1–3] as targets. In this work we investigate deformation effects in the one neutron pickup reactions at bombarding energies below the Coulomb barrier. For this purpose we use targets with different nuclear shapes, such as the spherical ^{144}Sm and the quadrupole-deformed ^{166}Er. The one-neutron transfer channel is particularly appropriate for this study since one does not have to consider sequential processes and Coulomb effects.

The relevant cross sections were determined via the analysis of delayed x-ray activities. This technique (see, for example, [4]), which was previously used to determine fusion reaction cross sections, was successfully extended in the present work to transfer reactions. Details of the experimental setup are described in Sec. II. The analysis and interpretation of the experimental results are given in Sec. III.

II. EXPERIMENTAL METHOD

Measurements were carried out at the 20-MV tandem accelerator of the TANDAR Laboratory in Buenos Aires. Enriched targets of ^{144}Sm and ^{166}Er with thickness of 110 and 92 $\mu g/cm^2$, respectively, were bombarded with ^{32}S projectiles with energies ranging from 123.5 to 152.5 MeV. The Coulomb barriers in the laboratory frame were estimated to be 136 MeV for $^{32}S + ^{144}Sm$ and 139 MeV $^{32}S + ^{166}Er$.

For both systems, transfer cross sections as a function of the bombarding energy have been determined by measuring the activity of the delayed x rays emitted in the subsequent decay of the reaction products, with decay half-lives of 8.83 min (^{143}Sm) and 10.36 h (^{165}Er).

The targetlike transfer products were trapped on gold catcher foils placed behind the targets. The thickness of the gold foils (~10 mg/cm^2), the chosen geometry and the forward-peaked angular distributions of these fragments at near-barrier energies guarantee at least 99% efficiency for the collection of the desired particles. After irradiations of typically 2 h, the catcher foils were removed from the scattering chamber and placed in front of an x-ray counter in order to accumulate and record several off-line energy spectra as a function of time. For the ^{166}Er target at the lowest bombarding energies the irradiation time was set to 6 h due to the long half-life of ^{165}Er.

The energy resolution of the x-ray detector was 700 eV FWHM at 60 keV, and its absolute efficiency was 9.5% in the energy range of 30 to 80 keV. Two solid state detectors placed at $\pm 30°$ with respect to an auxiliary Au target were used for absolute cross sections normalization.

An off-line energy spectrum of $^{32}S + ^{166}Er$ at a bombarding energy of 143.5 MeV for a given time interval is shown in Fig. 1. This figure shows the different x-ray lines from atoms with different atomic numbers that are produced through the radioactive decays of the various transfer products.

Transfer cross sections were obtained by fitting the delayed x-ray activities via a minimization procedure. For this purpose, the time dependence of the $K\alpha$ x-ray yields for both parent and daughter activities is calculated from the known half-lives and absolute number of photons produced per decay of each isotope in each mass chain. Then

*Permanent address: Departamento de Física, Universidad Nacional de La Plata, 1900 La Plata, Argentina.

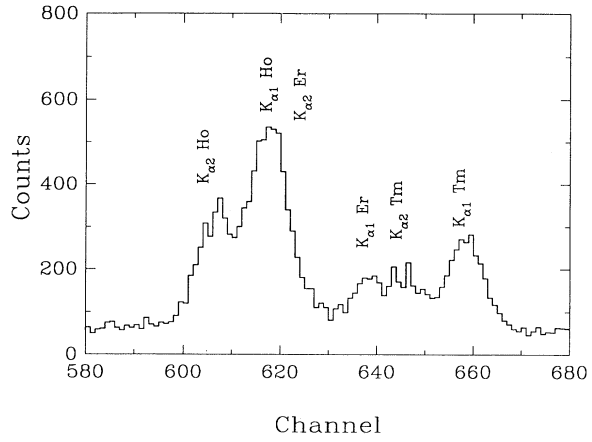

FIG. 1. Off-line energy spectrum following the $^{32}S + ^{166}Er$ reaction at a bombarding energy of 143.5 MeV. X-ray lines from different transfer channels are shown.

the transfer cross sections were deduced by minimizing the χ^2 function constructed from the experimental x-ray activities and the theoretical calculations [5].

Figure 2 shows the off-line time dependence of the activities for $^{32}S + ^{166}Er$ for an impinging energy of 143.5 MeV, together with the best fit to the data.

III. RESULTS AND DISCUSSION

The total one neutron pickup reaction cross sections for the two systems as a function of the laboratory energy are summarized in Table I and Fig. 3. The data points show the usual behavior for transfer reactions at subbarrier energies, namely, an almost exponential fall characteristic of a tunneling process.

Analysis of delayed x-ray activities show the presence of additional transfer channels. Cross sections for these channels are given in Table II.

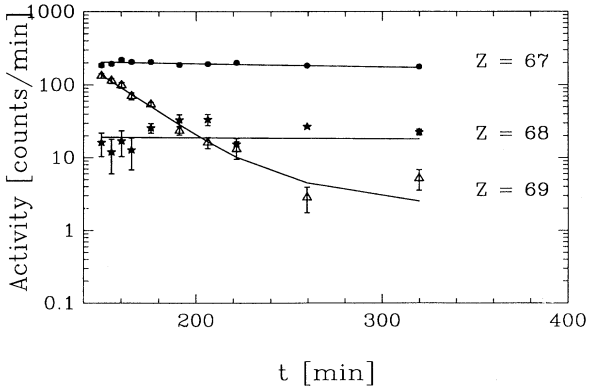

FIG. 2. X-ray activities for the $^{32}S + ^{166}Er$ reaction at a bombarding energy of 143.5 MeV. Solid lines are fit to the data.

TABLE I. Cross sections for one neutron pickup reaction in the systems $^{32}S + ^{144}Sm$ and $^{32}S + ^{166}Er$.

E_{lab}[MeV]	Total cross section [mb]	
	$^{32}S + ^{144}Sm$	$^{32}S + ^{166}Er$
124.5		2.4 ± 0.2
127.5		3.1 ± 0.5
130.5	2.7 ± 0.4	5.6 ± 0.5
131.5	3.5 ± 0.6	
132.5	4.9 ± 0.6	
133.5	4.5 ± 0.7	8.3 ± 0.8
134.5	6.8 ± 0.7	
135.5	7.1 ± 0.7	
136.0		12.5 ± 1.0
136.5	8.2 ± 0.7	15.9 ± 3.0
137.5		16.4 ± 2.0
138.5	10.1 ± 0.8	
140.5		20.0 ± 3.0
142.5		26.0 ± 3.0
143.5	24.7 ± 1.5	31.7 ± 4.5
144.5		33.0 ± 3.0
146.5	32.2 ± 2.0	
148.5		50.8 ± 3.6
150.5	48.5 ± 2.5	
152.5		65.2 ± 3.0

A. Semiclassical description of transfer probabilities

In a semiclassical approach the differential transfer cross section at energies below the barrier is given by [6]

$$\left(\frac{d\sigma}{d\Omega}\right)_{tr} = P_{tr}(\theta)\left(\frac{d\sigma}{d\Omega}\right)_{Coul}, \tag{3.1}$$

where $(d\sigma/d\Omega)_{Coul}$ denotes the differential cross section for Rutherford scattering and

$$P_{tr}(\theta) = \frac{\pi\kappa}{2\eta k} C_{AB} \sin\left(\frac{\theta}{2}\right) \exp\{-2\kappa d(\theta)\} \tag{3.2}$$

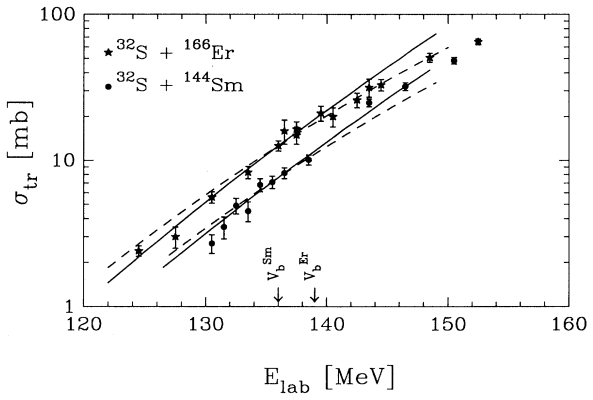

FIG. 3. Total one neutron transfer cross sections for the $^{32}S + ^{144}Sm$ and $^{32}S + ^{166}Er$ reactions as a function of E_{lab}. Dashed lines are calculations using expression (3.2) and solid lines are theoretical calculations obtained from (3.10). The arrows indicate the values of the Coulomb barrier for those systems.

TABLE II. Additional transfer channels observed in the ^{166}Er+^{32}S and ^{144}Sm+^{32}S systems.

System	Channel	Energy (LAB) [MeV]	Total cross section [mb]
^{166}Er+^{32}S	$2p$-$1n$	140.5	1.7 ± 0.2
		142.5	2.7 ± 0.3
		144.5	4.3 ± 0.2
		146.5	5.0 ± 0.2
		150.5	8.5 ± 0.4
^{144}Sm+^{32}S	$2n$	135.5	0.28 ± 0.08
		136.5	0.7 ± 0.2
		140.5	2.4 ± 0.3
		146.5	5.6 ± 0.6
^{144}Sm+^{32}S	$2p$	135.5	0.8 ± 0.3
		140.5	1.2 ± 0.3
		146.5	1.6 ± 0.2

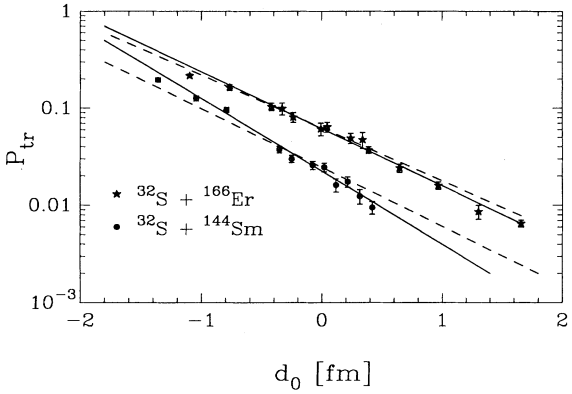

FIG. 4. Transfer probability P_{tr} as a function of the distance between effective nuclear surfaces for ^{32}S + ^{144}Sm and ^{32}S + ^{166}Er systems. Solid lines are fits to the data and dashed lines correspond to a slope calculated by expression (3.3).

is the transfer probability expected for nucleon tunneling between two potential wells as a function of the scattering angle θ. The amplitude C_{AB}, which will be discussed below, depends on the initial and final states as well as on the kinematics of the reaction (following the notation of Bass [6], A and B indicate the projectilelike and target fragments, respectively). In this expression k and η are the asymptotic wave function number and the Sommerfeld parameter of relative motion, respectively. The value of the propagation number κ is defined through the binding energy $\mathcal{B}$ of the transferred particle and its reduced mass μ as

$$\kappa = \left(\frac{2\mu\mathcal{B}}{\hbar^2}\right)^{1/2} . \tag{3.3}$$

The quantity d is the distance between the effective nuclear surfaces relevant to the occurrence of transfer

$$d = D - R_c , \tag{3.4}$$

where D is the distance of closest approach between the colliding nuclei and $R_c = 1.54\,(A_1^{1/3} + A_2^{1/3})$ fm [7] the interaction radius. Assuming Coulomb trajectories D is given by

$$D = \frac{D_0}{2}\left(1 + \csc\frac{\theta}{2}\right) , \tag{3.5}$$

where $D_0 = e^2\, Z_1 Z_2 / E_{\text{c.m.}}$ is the distance of closest approach in a head-on collision.

The transfer probability P_{tr} can be related to the total cross section σ_{tr} by integration of expression (3.1) over Ω using (3.2)

$$P_{tr}(d_0) = \sigma_{tr}\frac{2\kappa}{\pi\,(d_0 + R_c)} \tag{3.6}$$

with $d_0 = D_0 - R_c$. Therefore the transfer probability P_{tr} can be interpreted as a ratio between σ_{tr} and an "effective peripheral area" $\pi D_0/2\kappa$. This expression was used to construct a plot P_{tr} vs d_0 from measured cross sections (see Fig. 4). The full lines in this figure are fits to the data obtained with an exponential dependence of P_{tr} vs d_0. The corresponding slopes in the logarithmic plots are 0.91 fm^{-1} for ^{144}Sm and 0.67 fm^{-1} for ^{166}Er. In the last case the slope is consistent with the value obtained from (3.3). In the case of ^{144}Sm the experimental slope is not coherent with the binding energy. It is interesting to note that these results seem to be in contradiction with those of Betts [8]. This author finds agreement with the slopes determined from the binding energies for the spherical ^{144}Sm and not for the deformed ^{154}Sm. Besides the fact of the difference in the systems we do not have an explanation for this apparent discrepancy.

A more realistic treatment of the transfer process can be achieved from an extension of a model developed by Brosa and Gross [9], which includes a centrifugal term in the potential and considers that the transfer processes can also take place at distances larger than the distances of closest approach. In this description, the neutron being transferred moves along the line of centers under the influence of the combined potentials created by the donor and acceptor cores:

$$U(D,r) = U_1(r) + U_2(D - r) . \tag{3.7}$$

Now D is the distance between the cores 1 and 2, and r indicates the spatial coordinate of the transferred particle with respect to the donor core. In this approach, the neutron potential is given by

$$U_i(r) = \frac{V_i^0}{1 + \exp\left[(r - R_i)/a\right]} + \frac{l_i(l_i+1)\hbar^2}{2\mu_i r^2} , \tag{3.8}$$

where R_i, a, and l_i are the core radius, the diffuseness, and the relative angular quantum number of the nucleus i, respectively.

The nuclear potential depths V_i^0 were obtained as adjustable parameters from the numerical solution of Schrödinger's equation by requiring agreement between the theoretical and experimental binding energies [10]. The quantum numbers of these wave functions were the corresponding for the ground state, namely, $n = 2$; $l = 2$

and $n = 2$; $l = 3$ for ^{143}Sm and ^{165}Er, respectively, where n is the number of nodes minus one. For the calculations performed in the present analysis, we have taken $R_i = 1.27A_i^{1/3}$ fm and $a = 0.67$ fm (Ref. [9]).

In order to consider all possible transfer processes we proceeded as follows. Starting from the instantaneous one-dimensional tunneling probability

$$\frac{dP}{dt} \propto \exp\left(-2\int_0^d \kappa(r,l,t)\,dr\right) \tag{3.9}$$

at a fixed distance R between the two cores, and assuming Coulomb trajectories, the transfer probability results from a time integration over the trajectories for all relative angular momentum l of the cores properly weighted by the impact parameter b_l,

$$P_{\rm tr} = 2\pi\Lambda\, g_\lambda \sum_l b_l \int_{-\infty}^{\infty} dt \frac{dP}{dt}$$

$$= 2\pi\,\Lambda\, g_\lambda \sum_l b_l \int_{-\infty}^{\infty} dt\, \exp\left(-2\int_0^d dr\kappa(r,l,t)\right) \tag{3.10}$$

Λ being a normalization constant and the function $g_\lambda(Q)$ a correction due to mismatch of both angular momentum transfer λ and Q values [11]:

$$g_\lambda(Q) = \frac{1}{\pi}\int_0^\pi d\theta \exp\left[-\frac{1}{2}\left(\frac{Q-Q_{\rm opt}}{\gamma} - \frac{\hbar^2(l_g+\frac{1}{2})\lambda}{\gamma\mu R_i^2}\cos\theta\right)^2\right]. \tag{3.11}$$

In this expression the variance γ of the Q window was taken from Ref. [12] as $\gamma = 5.9$ MeV. The quantities $Q_{\rm opt}$ and l_g are the optimum Q value and the grazing angular momentum, respectively.

The quality of the agreement produced by this calculation is illustrated in Fig. 3. The solid curves are the calculated total transfer cross sections obtained using Eqs. (3.1), (3.5), and (3.10). The normalization constant Λ was used to adjust the data and takes a value of 0.025 for ^{144}Sm and 0.061 for ^{166}Er.

The improvement in the description of the data when using expression (3.10) compared to (3.2) can be understood as follows: On the one hand, the use of a more realistic potential (i.e., a Woods-Saxon potential) produce a significant change in the barrier shape (almost parabolic rather than square), specially at the smallest distances. This fact leads to an increase of the slope compared to that obtained from expression (3.3). On the other hand, the integration over all impact parameters give rise to a non-negligible modification with respect to the calculation assuming just head-on collisions specially at energies above the barrier.

B. Effects of nuclear deformation

The choice of a spherical projectile and the well-known structural characteristics of the ^{144}Sm and ^{166}Er are necessary ingredients if we attempt to study the effects of nuclear deformation.

Within a simple picture [1,2] the effect will show up through an enhancement of the transfer cross sections similar to that observed in subbarrier fusion but less pronounced because of the different kind of tunneling processes involved. Following Ref. [2] at low bombarding energies we expect an enhancement factor of about 2 between the transfer cross sections of ^{144}Sm and ^{166}Er, considering a deformation parameter of $\beta_2 = 0.34$ for ^{166}Er [13].

In order to derive an enhancement factor from the experimental data we need to remove effects not related directly to deformation. For this purpose we use the quantity $\mathcal{E}$ defined as the ratio of the transfer probability $P_{\rm tr}$ between the deformed and the spherical systems [given by the ratio between the constants Λ in (3.10)] properly normalized by the geometrical factors C_{AB},

$$\mathcal{E} = \left(\frac{\Lambda\eta}{C_{AB}\kappa}\right)_{\rm Er} \Big/ \left(\frac{\Lambda\eta}{C_{AB}\kappa}\right)_{\rm Sm} \tag{3.12}$$

with C_{AB} given by [6]

$$C_{AB} = \frac{N_A^2 N_B^2 S_A S_B}{\kappa_1^3\kappa_2^3}\frac{\mu_i\mu_f}{\mu_A\mu_B}\frac{2I_B+1}{(2I_2+1)(2j+1)}, \tag{3.13}$$

where μ_i and μ_f are the reduced mass of the initial and final systems and μ_A and μ_B are the reduced mass of the neutron in the cores A and B. The angular momentum quantum numbers I_2, I_B, and j correspond to the target-like fragment, to the target nucleus, and to the neutron, respectively. The factors N_A and N_B are normalization constants between the exact numerically determined neutron wave functions and the spherical Hankel functions that describes their asymptotic behavior. The quantities S_A and S_B are the spectroscopic factors of the cores, and $\kappa_{1,2}$ are given by

TABLE III. Enhancement factor $\mathcal{E}$ calculated using (3.12) for different values of the diffuseness and spectroscopic factors.

a [fm]	$N_{\rm Sm}^2$	$N_{\rm Er}^2$	$S_{\rm Sm}$	$S_{\rm Er}$	$\mathcal{E}$
0.65	2753	355	1.0	1.0	1.7
				0.5	3.4
			0.5	0.7	1.2
0.67	2688	373	1.0	1.0	1.7
				0.5	3.4
			0.5	0.7	1.2
0.70	2872	400	1.0	1.0	1.7
				0.5	3.4
			0.5	0.7	1.2

$$\kappa_{1,2} = \left(\frac{2\mu_{A,B}\mathcal{B}_{A,B}}{\hbar^2} \right)^{1/2} . \quad (3.14)$$

In this way, we could in principle remove all the structure and kinematic factors that appear in the expression of the transfer probability $P_{\rm tr}$, remaining only the dependence on the shape of the nuclei.

In spite of the uncertainties in some of the quantities entering in expression (3.13) (for example, the spectroscopic factors, and the wave function normalization constant N through its dependence on the nuclear diffuseness a) for realistic values related to neutron transfer to ground states both in ^{144}Sm and ^{166}Er we can derive an enhancement factor of $\mathcal{E} \approx 2$ (see Table III). This indicates an enhanced tunneling probability, that could be attributed to the quadrupole deformation of ^{166}Er.

IV. SUMMARY

Pickup transfer reactions in the ^{32}S + ^{144}Sm and ^{166}Er systems were measured at incident energies close to the Coulomb barrier. The transfer probability can be understood as a classical tunneling process between a donor and acceptor core. The experimental enhancement factor of the deformed ^{32}S + ^{166}Er system with respect to the spherical ^{32}S + ^{144}Sm system is consistent with that obtained from a simple semiclassical model.

Some of us (J.O.F.N., A.J.P, J.E.T., D.D.G., and C.P.M.) acknowledge the financial support of the Consejo Nacional de Investigaciones Científicas y Técnicas, Argentina.

[1] A.J. Pacheco, A.O. Macchiavelli, D. Abriola, D.E. Di Gregorio, A. Etchegoyen, M.C. Etchegoyen, J. Fernández Niello, A.M. Ferrero, S. Gil, J.A. Kittl, and J.E. Testoni, Z. Phys. A **331**, 451 (1988).

[2] S. Landowne and C.H. Dasso, Phys. Lett. B **202**, 31 (1988).

[3] J. Fernández Niello, J. Testoni, M. di Tada, A.J. Pacheco, D.R. Napoli, A.M. Stefanini, L. Corradi, B. Million, M. Narayanasamy, P. Spolaore, S. Beghini, G. Montagnoli, F. Scarlassara, G.F. Segato, C. Signorini, and F. Soramel, Phys. Rev. C **45**, 748 (1992).

[4] D.E. Di Gregorio, M. di Tada, D. Abriola, M. Elgue, A. Etchegoyen, M.C. Etchegoyen, J.O. Fernández Niello, A.M.J. Ferrero, S. Gil, A.O. Macchiavelli, A.J. Pacheco, J.E. Testoni, P.R. Silveira Gomes, V.R. Vanin, R. Liguori Neto, E. Crema, and R.G. Stokstad, Phys. Rev. C **39**, 516 (1989).

[5] A.J. Pacheco, D.E. Di Gregorio, J.O. Fernández Niello, and M. Elgue, Comput. Phys. Commun. **52**, 93 (1988).

[6] R. Bass, *Nuclear Reactions with Heavy Ions* (Springer-Verlag, Berlin, 1980).

[7] D.E. Di Gregorio, J. Fernández Niello, A.J. Pacheco, D. Abriola, S. Gil, A.O. Macchiavelli, J. Testoni, P. Pascholati, V.R. Vanin, R. Liguori Neto, N. Carlin Filho, M.M. Coimbra, P.R. Silveira Gomes, and R.G. Stokstad, Phys. Lett. B **176**, 322 (1986).

[8] R.R. Betts, in *Proceedings of the Symposium on Heavy Ion Interaction Around the Coulomb Barrier,* edited by C. Signorini *et al.*, Lecture Notes in Physics (Springer-Verlag, Berlin, 1988), Vol. 317, p. 93.

[9] U. Brosa and D.H.E. Gross, Z. Phys. A **298**, 91 (1980).

[10] M. Lederer and V.S. Shirley, *Table of Isotopes,* 7th ed. (Wiley, New York, 1978).

[11] R.A. Broglia, G. Pollarolo, and A. Winther, Nucl. Phys. **A361**, 307 (1981).

[12] A.M. Van Der Berg, K.E. Rehm, D.G. Kovar, W. Kutschera, and G.S. Stephans, Phys. Lett. B **194**, 3 (1987).

[13] S. Raman, C.H. Malarkey, W.T. Milner, C.W. Nestor, Jr., and P.H. Stelson, At. Data Nucl. Data Tables **36**, 1 (1987).